Molecular dynamics of linear and branched alkanes

Maurizio Mondello and Gary S. Grest

Citation: The Journal of Chemical Physics **103**, 7156 (1995); doi: 10.1063/1.470344
View online: http://dx.doi.org/10.1063/1.470344
View Table of Contents: http://scitation.aip.org/content/aip/journal/jcp/103/16?ver=pdfcov
Published by the AIP Publishing

Molecular dynamics of linear and branched alkanes

Maurizio Mondello and Gary S. Grest
Corporate Research Science Laboratories, Exxon Research and Engineering Company, Annandale, New Jersey 08801

(Received 9 May 1995; accepted 23 June 1995)

We have extended a recently introduced united atom model of *n*-alkanes to investigate the liquid-state dynamics of squalane, a molecule with six, symmetrically placed, methyl side groups. We compare our results with experimental measurements of diffusion in the same system and with experimental and simulation results on *n*-decane and *n*-tetracosane. The model reproduces the significantly different temperature dependence of diffusion in squalane and *n*-alkanes of similar mass. The results of a detailed comparative study of the intrachain local dynamics in the different molecules makes apparent its correlation with global single-chain relaxation processes. For linear alkanes, we also make a comparison between united atom and asymmetric united atom models. © *1995 American Institute of Physics.*

I. INTRODUCTION

There is significant practical interest in medium size alkanes (C_{20}–C_{40}) as the main constituents of lubricant base stocks. While here we are interested in liquid-state behavior, linear alkanes in this carbon range are solid at room temperature (*n*-paraffine waxes) and constitute a valuable byproduct of lubricant manufacturing.[1] Alkanes in this mass range represent also the simplest physical system for investigating the Rouse regime of polymer dynamics. Our main goal here is to characterize and correlate the structure and dynamics of medium size alkanes, partly as a test of the ability of presently available models to provide quantitatively reliable information beyond the more often investigated range of short alkanes. For this reason, we compare results obtained using two recently introduced models for *n*-alkanes.[2,3] Both models, which we will designate as *A* and *B*, use a spherical united atom (UA) potential to represent the nonbonded interaction, but the second model (*B*), proposed by Padilla and Toxvaerd,[3] introduces a displacement between the centers of force of nonbonded interaction and the centers of mass of the united atoms [asymmetric united atom (AUA)]. Models *A* and *B* also differ in the choice of torsional potential. We chose these two models because they have been successful in describing *n*-alkanes properties in other parts of phase space and we wanted to compare them under a set of conditions for which they had not being specifically optimized. Siepmann *et al.* have shown that model *A* quantitatively describes the liquid-gas boundary of the *n*-alkanes phase diagram,[2] including medium size alkanes at moderate densities, while model *B* was optimized to describe the static and dynamic behavior of short *n*-alkanes (C_5–C_{10}) at high pressure and temperature.[3] We consider here equilibrium properties and diffusion processes of medium size alkanes occurring under normal pressure and in a temperature range close to the melting point. The corresponding liquid densities are comparable to those found under high-temperature, high-pressure conditions.

To begin to investigate the effect of branching we have studied the equilibrium and dynamical properties of squalane (2,6,10,15,19,23 hexamethyl-tetracosane), a molecule with a C_{24} backbone and six, symmetrically placed, methyl side groups. This molecule is one of the few commercially available branched isoparaffines in the mass range of interest and has been used as a model system in boundary lubrication studies.[4] For the simulation of squalane we have used a direct extension of the model *A* potential used for linear alkanes and the calculated diffusion coefficients were compared with pulsed-field-gradient (PFG) nuclear magnetic resonance (NMR) results. At room temperature, diffusion in squalane is among the slowest relaxation processes investigated to date using chemically realistic models of liquids.

In Sec. II we describe the different models investigated and give details on the algorithmic implementation. The equilibrium results, with an emphasis on molecular geometry, are presented in Sec. III. We consider translational and rotational diffusion in Sec. IV, while, in Sec. V we give a detailed description of intramolecular dynamics and stress its correlation with global relaxation processes. Our conclusions are collected in Sec. VI.

II. MODELS

In all the alkane models considered hydrogens atoms are not explicitly simulated, but we distinguish between the different CH_n groups. These groups (united atoms) interact through bonded and nonbonded forces. The bonded interactions are represented by constraint forces which keep intramolecular nearest neighbors at a fixed distance (no explicit bond-stretching term is present), a bending term

$$V_b(\theta) = -\frac{k_b}{2}(\theta - \theta_b)^2, \tag{1}$$

where θ_b is the equilibrium angle between successive bonds, and a torsional term

$$V_t(\phi) = \sum_i a_i[\cos(\phi)]^i \tag{2}$$

characterizing preferred orientations and rotational barriers around all nonterminal (single) bonds. The nonbonded forces are described by Lennard-Jones (LJ) interaction sites located at the position of each carbon atom center of mass (model *A*, UA) or displaced in the direction of the full CH_n group cen-

 0021-9606/95/103(16)/7156/10/$6.00

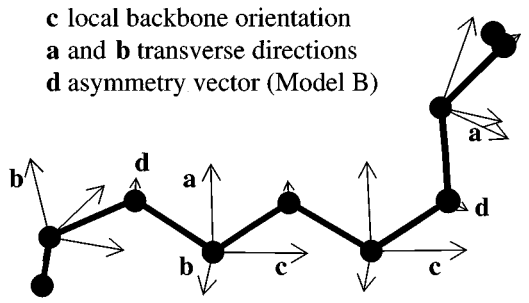

FIG. 1. Local reference frames (**a**,**b**,**c**) and AUA displacement vectors (**d**) at selected sites of model *n*-decane molecule. Meaning of vectors explained in the text.

ter of mass (model *B*, AUA). This displacement is meant to partially account for the anisotropy of interaction between CH_n groups, due to the hydrogens, which is neglected in the usual united atom representation. In Fig. 1 we show (in scale) the displacement vectors (**d**) on alternate sites of our model *n*-decane. The nonbonded Lennard-Jones potential is defined as

$$V_{\mathrm{LJ}}(r)=4\epsilon[(\sigma/r)^{12}-(\sigma/r)^{6}] \tag{3}$$

which has a minimum at $r_0=2^{1/6}\sigma$. We allow for both intermolecular and intramolecular nonbonded interactions except for sites which are connected by less than four bonds, and which therefore interact through one or more of the bonded interaction terms. Different LJ parameters are used for each CH_n group, see Table I. As shown in Table II, there is no essential difference in the bending potential for the two models,[5] but differences in the torsional potential should be noted. In comparison with the Jorgensen torsional potential[6] used in model *A*, the torsional potential of model *B* is characterized by a reduced barrier to gauche–gauche transition, a reduced energy difference between the gauche (g) and trans (t) states and an increased $t-g$ energy barrier (Fig. 2). The reduced separation between energy minima should increase the compactness (thermodynamic flexibility) of the molecular structure of model *B* relative to *A* and make it less sensitive to temperature variations. One might expect, however, the $t-g$ barrier height to be the determining factor in the kinetic of torsional rearrangement, enhancing the dynamical flexibility of model *A*. In order to single out the effect of the torsion, we have substituted the torsional potential of model

TABLE I. Lennard-Jones potential parameters.

Model	Group	σ (Å)	ϵ (K cal/mol)	d (Å)
A (UA[a])	CH_3	3.930	0.227	
	CH_2	3.930	0.093	
	CH	3.810	0.080	
B (AUA[b])	CH_3	3.527	0.238	0.275
	CH_2	3.527	0.159	0.159

[a]The parameters for *n*-alkanes are taken from Ref. 2 and the parameters for CH are close to the parameters in Ref. 6.
[b]This is model $AUA_{(2)}$ from Ref. 30.

TABLE II. Intramolecular interaction parameters.

	Model *A* (UA[a])	Model *B* (AUA[b])	Units
Bond length	1.54	1.54	Å
k_b (bending)	124.28	124.18	Kcal/(mol rad^2)
θ_b	114°	114.6°	deg.
k_i (sp_3) bending	40.0		Kcal/(mol rad^2)
θ_i	27.25°		deg.
a_0 (X–CH_2–CH_2–Y)	2.007	2.062	Kcal/mol
a_1	4.012	4.821	
a_2	0.271	0.162	
a_3	−6.290	−6.218	
a_4		−0.324	
a_5		−0.502	
a_0 (X–CH_2–CH–Y)	0.814		Kcal/mol
a_1	1.792		
a_2	0.389		
a_3	−3.673		

[a]Intramolecular parameters for *n*-alkanes from Ref. 2. Torsional potentials are taken from Ref. 6.
[b]Intramolecular parameters from Ref. 30. The torsional potential (d) from the same reference was used.

B in the parameter set of model *A* (model A_1) and the torsional potential of model *A* in the parameter set of model *B* (model B_1).

The previous considerations apply to both linear and branched alkanes, but for our extension of model *A* to branched hydrocarbons a few additional points should be noted. We have chosen LJ parameters for the CH group close to the parameters in Ref. 6, but we did not distinguish between methyl groups attached to secondary and tertiary carbons. While our potential is not specifically optimized for branched alkanes,[7] we wanted to use as close a model as possible for the linear and branched molecules in order to make a more significant comparative study of the effect of structure on physical properties. Furthermore, presently available UA potentials for general alkanes do not seem to provide adequate parameters for branched alkanes in the

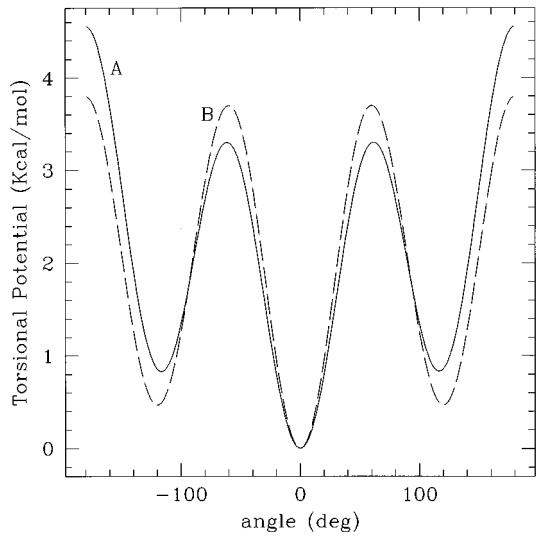

FIG. 2. Comparison of torsional potential around X–CH_2–CH_2–Y type bonds for models *A* and *B*.

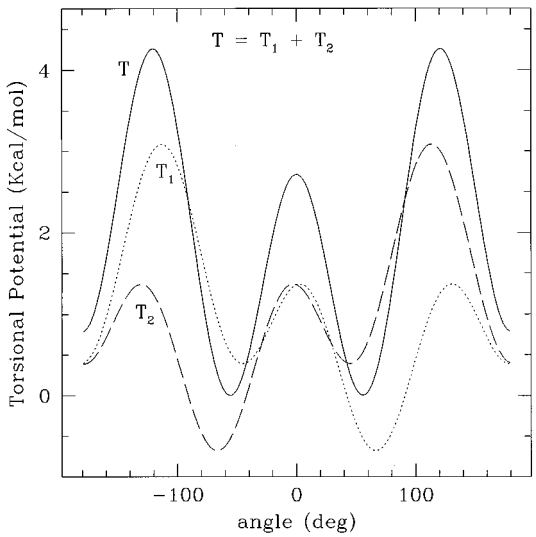

FIG. 3. Decomposition of torsional potential around X–CH–CH_2–Y type bonds. Two identical potentials are assigned, with an appropriate shift, to the two quadruplets of united atoms bearing on each bond.

mass range of interest.[8] The spherical averaging of the LJ interaction potential which is implied when going from a full atom to a UA description, makes it difficult to separate the effective hindrance to rotation around nonterminal single bonds into an intrinsic torsion contribution and a LJ contribution. Therefore, rather then trying to introduce *ad hoc* LJ parameters for this purpose, we have chosen to extend the use of effective torsional potentials, typical of simulations of linear alkanes, to the branched case. For the present simulations we only need to specify torsional potentials around two types of bonds: X–CH_2–CH_2–Y and X–CH–CH_2–Y, where we are ignoring the nature of the X and Y groups. For these two we have used literature parameters,[6] but we are developing parameters for the remaining four cases.[9] It should be noted that an effective potential is defined for the bond rather than for the quadruplet(s) of (united) atoms that bear on that bond. It is possible, however, to decompose the potential among the quadruplets,[10] but in doing so care should be taken of the fact that the decomposition will depend on the values chosen for the equilibrium bending angles (see Fig. 3). Finally, an *ad hoc* harmonic potential, similar to the bending term, is introduced to prevent umbrella inversion of the sp_3 bond configuration at tertiary carbon branch points (see Table II). This potential forces the normal to the plane defined by the two backbone bonds joining at the CH group to oscillate around its equilibrium position, which forms an angle of 27.25° with the normal to the plane defined by the three CH_n groups connected to the tertiary carbon (the direction of the missing C–H bond). The exact value of this equilibrium angle also depends on the values of the bending angles.

All the results presented here were obtained by constant volume simulations, using experimental densities at 0.1 MPa. We have run both microcanonical (*n*-decane) and constant *T* (for the other molecules) simulations using 2.5 and 5 fs time steps, respectively. The velocity rescaling algorithm

TABLE III. Substances and state points simulated.

Substance	T (K)	ρ[a] (g/cm^3)	Run (ns)
n-decane	298	0.7247[b]	2.0
n-tetracosane	333	0.7728	1.5
	372	0.7475	1.2
	405	0.726[c]	1.0
squalane	293	0.8100[d]	5.0
	311	0.7979	4.0
	333	0.7837	3.0
	372	0.7592	2.2

[a]Normal pressure densities obtained from Ref. 31, except when otherwise specified.
[b]Reference 32.
[c]Reference 21.
[d]Reference 33. The value reported in Ref. 31 is 0.8092.

of Berendsen *et al.*[11] was used in the constant *T* simulations. The bond length was kept constant using the RATTLE algorithm.[12] 64 (*n*-decane) and 100 (*n*-tetracosane, squalane) molecules were used and run length varied between 1 and 5 ns (see Table III). The reported run length does not include equilibration times that varied from a few hundred picoseconds for the *n*-alkanes to a few nanoseconds for squalane.

III. EQUILIBRIUM RESULTS

Selected results for the average equilibrium shape of *n*-tetracosane and squalane are presented in Table IV. A comparison of the results for *n*-tetracosane at 60 °C shows a significant difference in the radius of gyration (R_g) and the end-to-end distance (R_{ee}) for models *A* and *B*. It can also be seen that these differences are significantly reduced, as expected, when we compare models with the same torsional potential (models A_1 and *B*). Including in the comparison the results for model B_1 seems to indicate, however, that the UA model is less sensitive than the AUA model to changes in the torsional potential. This may reflect a stronger coupling between torsion and intrachain non-bonded interaction in the AUA model. In all cases we find a decrease of R_g with increasing temperature, together with a reduction in the degree of asymmetry in the molecule, as shown by a decrease of the largest eigenvalue (l_1^2) of the mass tensor.[13] These eigenvalues (l_i^2) satisfy the relation $l_1^2+l_2^2+l_3^2=R_g^2$. While model *B* results indicate a more compact structure at all temperatures considered, the effect of temperature seems to be more significant in model *A*. At nearby temperatures, the changes in the geometrical parameters are sometimes comparable with our statistical uncertainties. The small change over the entire temperature interval considered, however, can be used to obtain a rough estimate of the expansion coefficient $k=d(\ln R_g^2)/dT$. We obtain $k=-1.1\pm0.2$ and $-0.6\pm0.3\times10^{-3}$ K^{-1} for model *A* and *B* of *n*-tetracosane, respectively. A similar calculation for squalane gives $k=-0.9\pm0.2\times10^{-3}$ K^{-1}. The corresponding experimental value for bulk polyethylene is $k=-1.07\pm0.08\times10^{-3}$ K^{-1}, obtained from SANS measurements.[14] While more accurate estimates of the expansion coefficient would clearly be desirable, our present results suggest that the torsional potential

TABLE IV. Equilibrium results.

Substance	Model	T (K)	R_g^2 (Å^2)	l_1^2/R_g^2	l_2^2/R_g^2	R_{ee}^2 (Å^2)
n-decane	*A*	298	11.49(0.02)	0.920(0.001)	0.067(0.001)	97.1(0.3)
	B	298	10.72(0.04)	0.896(0.002)	0.086(0.001)	86.7(0.5)
n-tetracosane	A_1 [a]	333	44.0(0.3)	0.854(0.003)		357(5)
	A	333	48.9(0.4)	0.868(0.003)		409(6)
		372	46.3(0.3)	0.853(0.003)		376(5)
		405	45.3(0.3)	0.852(0.003)		367(5)
n-tetracosane	B_1 [b]	333	49.8(0.4)	0.871(0.003)		418(6)
	B	333	41.8(0.5)	0.836(0.005)		326(7)
		372	40.3(0.4)	0.827(0.004)		307(6)
		405	40.1(0.4)	0.833(0.004)		309(6)
squalane	*A*	293	49.4(0.6)	0.832(0.006)	0.137(0.005)	363(8)
		311	49.0(0.5)	0.835(0.005)	0.133(0.004)	363(7)
		333	46.8(0.4)	0.819(0.004)	0.146(0.003)	336(6)
		372	46.0(0.3)	0.818(0.003)	0.147(0.003)	329(4)

[a]For this calculation we substituted the torsional potential of model *B* in the parameter set of model *A*.
[b]For this calculation we substituted the torsional potential of model *A* in the parameter set of model *B*.

for linear alkanes used in model *B* underestimates the energy difference between the trans and gauche minima.

A comparison of the results for squalane and *n*-tetracosane (model *A*) at 60 °C and 99 °C shows that the model isoparaffine (Fig. 4), although more massive, presents a slightly more compact structure. This can be clearly seen in the smaller asymmetry and R_{ee} value for squalane, which has the same number of backbone carbons as *n*-tetracosane. This result points out that while the increased steric hindrance due to the small branches decreases the dynamic flexibility of the molecule, its compactness is actually increased. This fact is not directly reflected by R_g, which is sensitive not only to the overall chain conformation, but also to differences in local mass distribution along the chain backbone (the six extra methyl groups in squalane increase the weight of the chain ends with respect to its central region).

The values for the calculated pressure (P_{cal}) are collected in Table V. These should be compared with $P_{\mathrm{exp}}=0.1$ MPa (see Sec. II). For the *n*-alkanes we note that the error is of opposite sign but similar magnitude in models *A* and *B* and increases with n, in the range considered. The result for *n*-tetracosane (model *B*) is consistent with findings of Pant *et al.*,[15] who tested a very similar model for bulk polyethylene. There is only a small temperature dependence of P_{cal} in both models. The limitations of our model parameters for squalane can be clearly seen from both the size and temperature dependence of the calculated pressure, particularly when compared with *n*-tetracosane (model *A*). A small shift was observed between the pressure calculated from atomic positions (including constraint forces) and molecular center of mass (c.m.) positions. The main contribution to this shift comes from the virial and is timestep dependent (1–2 and 0.3–0.4 MPa with a 5 fs and a 2.5 fs time step, respectively). We have also calculated the pressure following the formulation of Honnell *et al.*[16] which uses atomic positions and a three-body contribution to the virial, but does not include intramolecular contributions. For both time steps considered, Honnell formulation gives essentially identical results (on average) to the pressure defined using molecular c.m. positions. This ''molecular'' pressure was reported in Table V with the associated statistical variation. We further discuss the significance of the pressure for model optimization in Sec. IV.

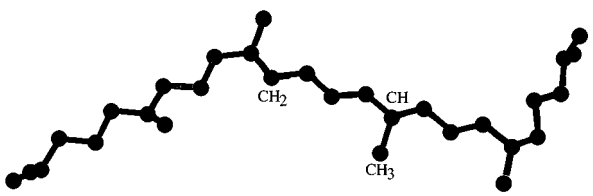

FIG. 4. Typical configuration for a squalane molecule in the bulk at 20 °C ($\rho=0.8100$ g/cm^3). This configuration radius of gyration, $R_g=7.04$ Å, and end-to-end distance, $R_{ee}=19.05$ Å, are very close to the time-averaged values for the entire system.

IV. DIFFUSION RESULTS

Calculated diffusion constants for the two models of linear alkanes investigated are collected in Table V. In all cases considered, model *B* gives lower diffusion values than model *A*, and the discrepancy increases for the lower values of the diffusion (lower T or longer molecule). A comparison is made with PFG NMR data obtained by Garcia and Silbernagel[17] in our laboratory and with literature data.[18] Model *B* gives consistently better results for *n*-decane and *n*-tetracosane. In order to check the effect of the difference in torsional potential between models *A* and *B*, we tested models A_1 and B_1 (*A* with *B* torsional potential and vice versa). The results in Table V seem to indicate that a torsional potential with lower $t-g$ barrier leeds to faster diffusion. We also note that for diffusion, as for the average molecular shape (see Sec. III), AUA models seem to be more sensitive than UA models to changes in the torsional potential. To correlate the differences in the diffusion results of models *A*

TABLE V. Diffusion results.

Substance	Model	T (K)	D_{cal} (10^{-6} cm^2/s)	D_{exp} [a]	P_{cal} (MPa)	Run (ns)
n-decane	*A*	298	16.0(0.5)	14.0[b]	−1.3(0.2)	2.2
	B	298	13.9(0.4)	14.0[b]	1.3(0.3)	2.0
n-tetracosane	A_1 [b]	333	3.87(0.15)	2.58	−13.4(0.6)	1.5
	A	333	4.50(0.17)	2.58	−10.8(0.6)	1.5
		372	8.50(0.38)	5.65	−9.2(0.4)	1.2
		405	12.90(0.89)	8.23	−8.2(0.3)	1.0
n-tetracosane	B_1 [c]	333	3.84(0.16)	2.58	8.7(0.4)	1.5
	B	333	2.70(0.11)	2.58	13.2(0.5)	1.5
		372	5.50(0.21)	5.65	13.8(0.3)	1.2
		405	8.90(0.62)	8.23	14.2(0.5)	1.0
squalane	*A*	293	0.31(0.02)	0.27	−70.4(0.7)	5.0
		311	0.62(0.03)	0.48	−66.2(0.6)	4.0
		333	1.50(0.11)	1.00	−62.1(0.6)	3.0
		372	3.39(0.11)	2.60	−55.0(0.3)	2.2

[a]Pulsed-field-gradient NMR results from our laboratories (Ref. 17). The overall uncertainty of the measured diffusion constants is estimated to be 10%
[b]Pulsed-field-gradient NMR results from Ref. 18 give 13.1.
[c]For this calculation we substituted the torsional potential of model *B* in the parameter set of model *A*.
[d]For this calculation we substituted the torsional potential of model *A* in the parameter set of model *B*.

and *B* with other single-chain dynamical properties of the two models, we compare in Fig. 5 the results for the correlation relaxations of the square end-to-end distance and the square radius of gyration of *n*-decane at 25 °C. The two quantities closely track each other in both models, but the relaxation is considerably faster (by almost a factor of 3) in model *A*, a direct confirmation of the enhanced dynamical flexibility of this molecular model.

The computed self-diffusion constants for squalane, also presented in Table V, overestimate experimental results by 15 to 50% over a temperature range where the diffusion rate changes by one order of magnitude. Note that for squalane we also find fairly large negative pressures. No attempt has been made here to introduce pressure corrections, which could roughly halve the calculated diffusion constants of our squalane model. For any given model, such a correction would give an estimate of the change of diffusion constant to be expected in a constant pressure ($P=0.1$ MPa) vs a constant volume simulation (where experimental densities are used), but this correction is of limited value when comparing different models. In fact, by appropriately modifying the LJ parameters, we can change the pressure while leaving the diffusion constant unchanged and vice versa.[19] The effect of such changes on other static and dynamical properties would

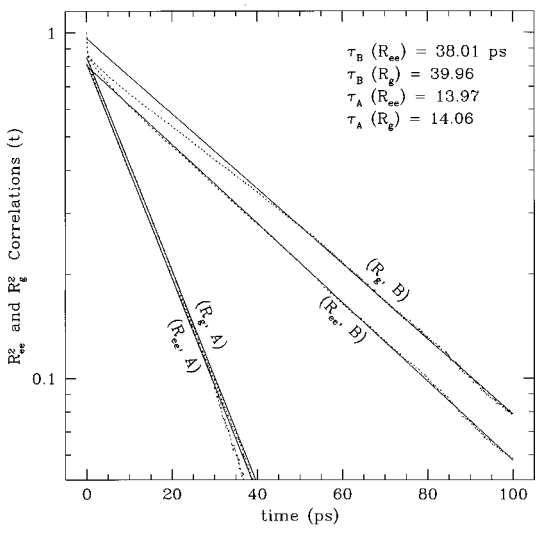

FIG. 5. Time correlations of the square end-to-end distance, R^2_{ee}, and the radius of gyration, R^2_g, for models *A* and *B* of *n*-decane at 25 °C.

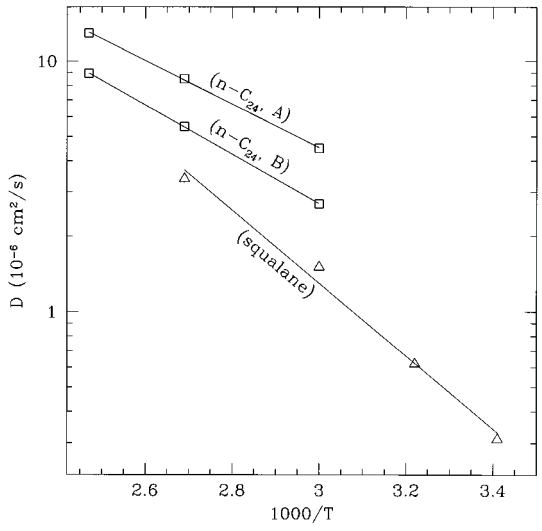

FIG. 6. Arrhenius plot of diffusion constant vs (inverse) temperature for *n*-tetracosane (models *A* and *B*) and squalane. From the linear fits shown, we calculate energy barriers of 3.98 and 4.50 Kcal/mol for models *A* and *B* of *n*-tetracosane, respectively, to be compared with a value of 4.04 Kcal/mol obtained from viscosity measurements[21] and a value of 4.36 Kcal/mol from the PFG NMR results.[17] The estimated energy barrier for squalane is 6.66 Kcal/mol, compared to 6.23 Kcal/mol from the PFG NMR data (Ref. 17).

have to be evaluated, but the fact remains that the magnitude or sign of the pressure correction does not unambiguously indicate how and how easily the model could be improved.

In the relatively small temperature range considered, self-diffusion can be adequately described by an Arrhenius-type equation (Fig. 6), characterized by a temperature-independent energy barrier.[20] The value of this energy is a direct measure of how fast the self-diffusion (and viscosity) changes with temperature. We find values of 3.98 and 4.50 Kcal/mol for models *A* and *B* of *n*-tetracosane, respectively, to be compared with a value of 4.04 Kcal/mol obtained from viscosity measurements[21] and a value of 4.36 from PFG NMR results.[17] For squalane, the energy barrier estimated from the computed diffusion values is 6.66 Kcal/mol compared to 6.23 Kcal/mol from the PFG NMR results.[17] The good agreement between calculated and experimental energy barriers suggests that the present simulations may offer a sound basis for investigating how molecular structure influences dynamical properties in longer alkanes. Here we simply note that the slightly higher energy barrier to self-diffusion calculated for model *B* of *n*-tetracosane, as compared to model *A*, seems to correlate with the reduced dynamical flexibility of the molecular model and higher $t-g$ barrier. These differences in dynamic flexibility can also help to explain the large variation in the temperature dependence of diffusion of squalane and *n*-tetracosane.

The reported statistical uncertainty for each diffusion constant was evaluated considering the variation of the time-averaged mean square displacement (msd) of the center of mass of the individual molecules in the system and assuming that the their motion becomes uncorrelated over the length of the run. Strictly speaking, this is therefore a lower bound and we expect it might underestimate the actual uncertainty by up to a factor of 2 for the slower diffusion range considered. A source of systematic error in the calculation is represented by a small positive difference (ca. 1%) between the molecular and the atomic kinetic temperatures.[22] Because the Berendsen algorithm keeps the atomic kinetic temperature very close to its target value, we can estimate, on the basis of experimental correlations for *n*-hexadecane,[23] that this temperature shift may increase the calculated diffusion constant by 2–3 %.[24] This change would be difficult to measure in our simulations, however, because it is smaller than our statistical uncertainties. While the problem could be reduced by decreasing the time step, the intrinsic limitations of the models considered, made evident, for example, by a comparison of calculated and experimental pressures, did not appear to warrant the substantial added computational effort. When considering slow diffusion processes, long transients are another potential source of systematic errors. It is important, therefore, to have some "*a priori*" criterion for deciding when the asymptotic behavior has been reached. For molecular diffusion one such criterion could be the requirement that the molecule has diffused at least (but preferably a few times) its own radius of gyration. Diffusion of squalane at room temperature is a case in point and Fig. 7 shows the averaged msd of the isoparaffine center of mass vs time at 20 °C (R_g^2 is also shown for comparison). For this particular run, the plot appears nearly linear from early times but a clear change in slope is visible at about 1 ns. This leads to a reduction of the estimated diffusion of about 20%. The linearity of the plot, by itself, would clearly be a poor criterion for establishing asymptotic behavior. While we cannot exclude (smaller) readjustments on a time scale 2–3 times longer than the one explored, it is interesting to note that 1 ns is also the time that characterizes the transient behavior of local reorientation at the center of the molecule (see Sec. V).

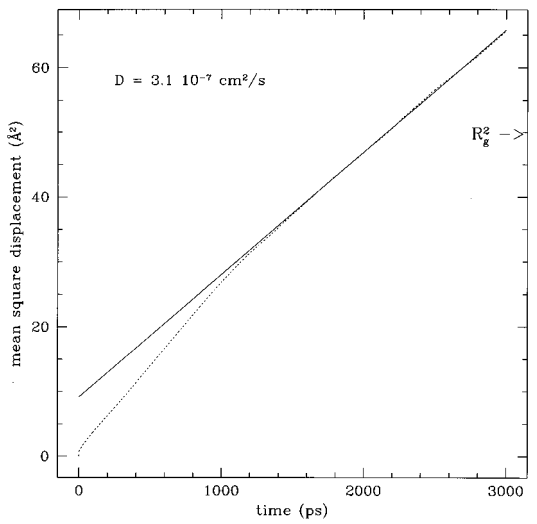

FIG. 7. Mean square displacement (msd) of squalane vs time at 20 °C. The diffusion constant from the terminal slope is $D=3.1\times10^{-7}$ cm^2/s. For comparison, we show the location of the average square radius of gyration, R_g^2, on the msd axis.

We have also considered the global rotational motion of the molecules. This can be characterized by the orientational relaxation of the longest principal axis of the molecule's ellipsoid of inertia ($\mathbf{e}_1$). Results are collected in Table VI, where τ_1 and τ_2 indicate the characteristic relaxation times of the first- and second-order angular correlation functions

$$P_1^{e_1}(t)=\langle \mathbf{e}_1(t)\cdot\mathbf{e}_1(0)\rangle \tag{4}$$

and

$$P_2^{e_1}(t)=\tfrac{1}{2}(3\langle[\mathbf{e}_1(t)\cdot\mathbf{e}_1(0)]^2\rangle-1). \tag{5}$$

In the case of isotropic rotational diffusion a value of 3 for the ratio τ_1/τ_2 is expected.[25,26] The characteristic times given for squalane at the lower temperatures can only be considered as rough estimates, since they describe processes occurring over a time scale as large as the total length of the simulation run, and no systematic error estimation is possible in this case. There are, however, some general considerations suggested by the data. In the temperature interval considered, the diffusion constant of squalane and the corresponding τ_1 vary by about 1 order of magnitude but their product remains essentially constant. In particular, $(6D\tau_1)^{1/2}$, the distance traveled by the molecule during an interval τ_1, remains close to 10 Å ($R_g\approx7$ Å). Analogous values are found for *n*-tetracosane. This suggests a significant coupling between translational and rotational diffusion. This claim is also supported by the low values of the τ_1/τ_2 ratio, which may indicate that the orientational relaxation of the molecule is spa-

TABLE VI. Rotational diffusion of molecular axis (e_1).

Substance	Model	T (K)	τ_1 [a] (ns)	τ_2 [a] (ns)	τ_1/τ_2	$(6D\tau_1)^{1/2}$ (Å)
n-decane	*A*	298	0.058	0.021	2.82	7.5
	B	298	0.051	0.019	2.68	6.5
n-tetracosane	A_1 [b]	333	0.516	0.229	2.25	10.9
	A	333	0.531	0.215	2.47	12.0
		372	0.211	0.092	2.29	10.4
		405	0.170	0.071	2.39	11.5
n-tetracosane	B_1 [c]	333	0.630	0.251	2.51	12.0
	B	333	0.580	0.281	2.06	9.7
		372	0.256	0.117	2.19	9.2
		405	0.173	0.078	2.22	9.6
squalane	*A*	293	5.72	2.56	2.23	10.3
		311	2.85	1.27	2.24	10.3
		333	1.12	0.49	2.29	10.0
		372	0.464	0.186	2.49	9.7

[a]An uncertainty of up to 10% can be expected in the reported values of τ_1 and τ_2.
[b]For this calculation we substituted the torsional potential of model *B* in the parameter set of model *A*.
[c]For this calculation we substituted the torsional potential of model *A* in the parameter set of model *B*.

tially constrained.[27] This ratio appears to increase with temperature with the notable exception of *n*-tetracosane (model *A*) close to the melting point. However, given the systematic[28] and statistical uncertainties in our data, no detailed conclusion on the temperature dependence can be reached.

V. INTRAMOLECULAR DYNAMICS

Because of the strong anisotropy in the local relaxation properties we analyze the intramolecular relaxation along the unit vectors of an embedded local frame, shown in Fig. 1 at a few positions of our model *n*-decane. The frame's axes identify the local orientation of the backbone (**c**), the perpendicular direction in the local plane of the molecule (**a**), and the direction perpendicular to the molecular plane (**b**). We have also considered the orientational relaxation of the **CH** bond vectors associated to secondary carbons. These vectors can be expressed as linear combination of **a** and **b**: $\mathrm{CH}_{\pm} = -\mathbf{a}\cos(54.75) + \mathbf{b}\sin(54.75)$.

In Fig. 8 we show a correlation between the global rotational relaxation of *n*-decane, characterized, as discussed in Sec. IV, by the relaxation of the orientation of its longest principal axis of inertia ($\mathbf{e}_1$), and the average relaxation of the of the equivalent pair of local **c** vectors at the center of the molecule. While the initial relaxation of the **c** vectors clearly shows the influence of rapid intramolecular processes, the relaxation of both the first and the second moment angular correlations of the **c** and $\mathbf{e}_1$ vectors track each other over a significant time interval, indicating that the two quantities are sensitive to the same global relaxation processes. In this instance, no significant differences were observed between models *A* and *B*. We also show, in the same picture, the second-order angular correlation of the central **CH** vectors. This is representative of the very fast relaxation observed for vectors in the (**a**,**b**) plane, but it also shows a correlation with global reorientation at later times. Correlated deviations from simple exponential behavior in the second-order angular correlations are also observed for $t \geqslant \tau_1$. At room temperature (25 °C), the ratio of the characteristic times of the first and second moment relaxation seems somewhat lower than 3, the value expected for a isotropically diffusive rotational process. In Fig. 9 we show that the same results hold also for *n*-tetracosane (at 99 °C), even though the characteristic relaxation times are here four times as large. The curves for the **c** and **CH** vectors represent here the average results over four vectors at the center of the molecule. The ratio of the time constants for the first and second moment relaxations is here clearly lower than 3. Deviations from simple exponential be-

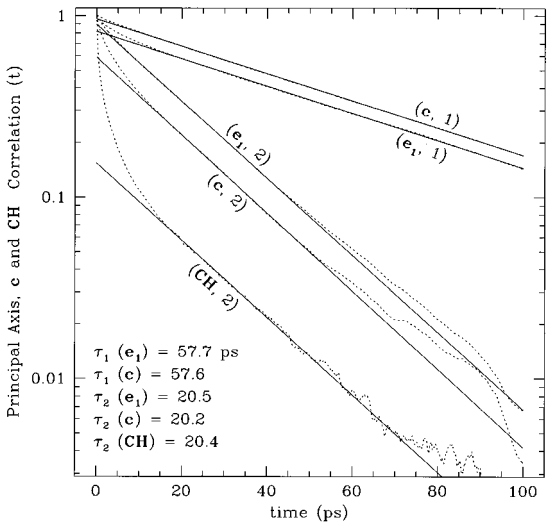

FIG. 8. Correlation between the global rotational relaxation of the (model *A*) *n*-decane molecule at 25 °C, characterized by the (first- and second-order) relaxation of the orientation of its longest principal axis of inertia, $\mathbf{e}_1$, and the average relaxation of the equivalent pair of local **c** vectors at the center of the molecule. The calculated ratios of first- and second-order relaxation times (τ_1/τ_2) are 2.82 and 2.83 for the $\mathbf{e}_1$ and the **c** vectors, respectively. Second-order angular correlation of the central **CH** bond vectors is also shown.

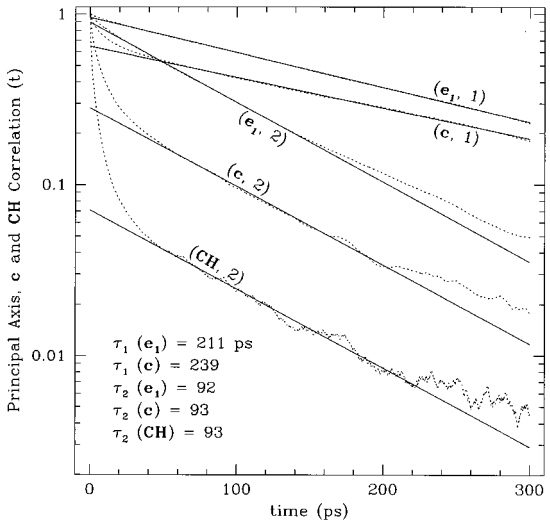

FIG. 9. Comparison of global (first- and second-order) rotational relaxation ($\mathbf{e}_1$) and local backbone reorientation (**c**) for model *A* of *n*-tetracosane at 99 °C. We find τ_1/τ_2 ratios of 2.29 and 2.55 for the $\mathbf{e}_1$ and the **c** vectors, respectively. Second-order **CH** bond reorientation is also shown. The local vectors reflect the relaxation at the center of the molecule.

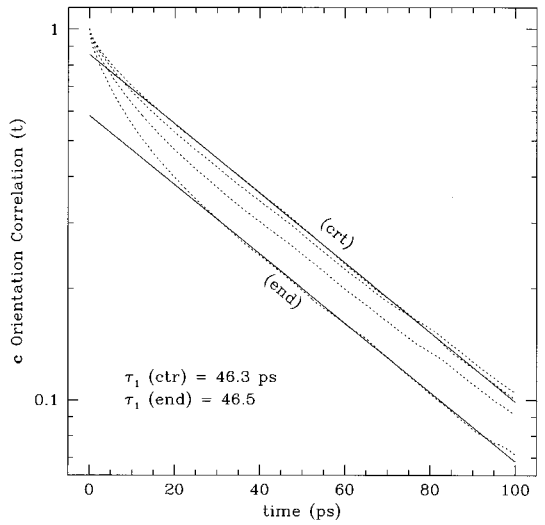

FIG. 11. First-order relaxation of the **c** vectors at different positions along the backbone for model *A* of *n*-decane at 25 °C.

havior at later times can again be observed for the second order angular correlations.

The first moment correlations of the **a** and **b** vectors at the center of the *n*-tetracosane molecule in models *A* and *B* are compared in Fig. 10. It should be noted that their orientation relaxes over a time scale 1 order of magnitude shorter than the orientation of the corresponding **c** vectors, while there is only a modest difference between **a** and **b**. Furthermore, the relaxation is significantly slower in model *B*. Notice that the relaxation behavior of the **a** and **b** vectors, as represented in Fig. 10, cannot always be adequately described by a simple exponential. It is useful, however, to associate a characteristic time to these processes as a guide to qualitative comparisons over a time range of interest.

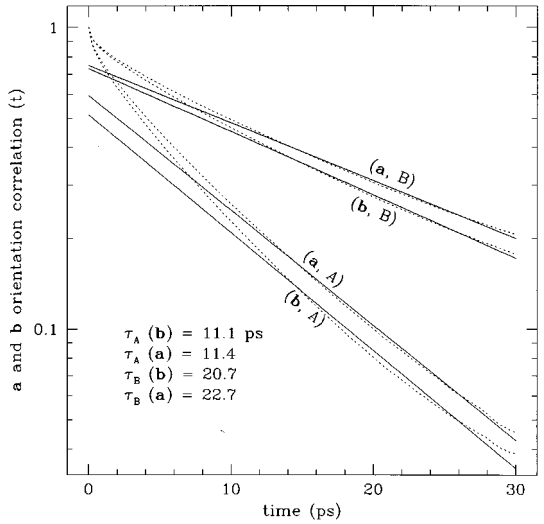

FIG. 10. First-order time correlations of the **a** and **b** unit vectors at the center of the *n*-tetracosane molecule at 99 °C. A comparison of models **A** and **B** results.

In Fig. 11, we consider the relaxation of the **c** vectors at different positions along the backbone of *n*-decane. There are in principle four equivalent pairs of **c** vectors and the four curves shown, averaged over each pair, clearly indicate that the initial relaxation is strongly influenced by the bond position, reflecting, as expected, an increased latitude of motion towards the ends of the molecule. Nevertheless, over a time scale comparable with the characteristic time of global rotational relaxation, all vectors follow the same decay law, indicating that the molecule retains a considerable degree of rigidity.

We compare the orientation relaxation of the **b** vectors at the center and at the ends of the *n*-decane and *n*-tetracosane in Fig. 12. We do not see any significant difference in *n*-decane, again pointing to a substantial degree of rigidity, while the large separation seen in *n*-tetracosane seems to indicate a significant degree of flexibility of the molecular ends. Note that the relaxation curves for *n*-decane (at 25 °C) fall in between the relaxation curves for *n*-tetracosane (at 99 °C), with only a moderate increase for the relaxation time of **b** vectors in the central region of the longer molecule. This should be contrasted with the relaxation of the central **c** vectors which shows a fourfold increase going from *n*-decane to *n*-tetracosane at the given state points. This increased separation of time scales between global and local motions and the interplay between them should be a guide in interpreting experimental relaxation results and may provide, at the same time, a more stringent test of force-field parameters.

A similar asymmetry between the relaxation of the **c** vectors and the transversal vectors **a** and **b** was seen in a simulation of a polyethylene melt.[27] In particular, the **c** vector relaxation became extremely sluggish for times larger than the characteristic relaxation time of the dihedral angle autocorrelation. Because end effects were eliminated from the model, no position dependence of the relaxation along

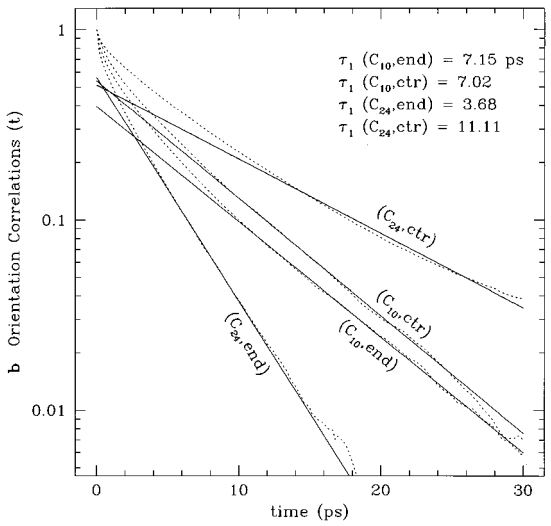

FIG. 12. First-order orientation relaxation of the **b** vectors at the center and at the molecular ends of *n*-decane (at 25 °C) and *n*-tetracosane (at 99 °C). Results for model *A*.

the chain (as discussed earlier) should be expected in this case. This result is consistent with our analysis and it seems to indicate that even for very long chains the relaxation of the local backbone orientation is sensitive to the large-scale reorientation processes of the chain.

At room temperature (20 °C), as seen in Table VI, the characteristic relaxation time for global rotation of the squalane molecule is about 2 orders of magnitude larger than for *n*-decane (at 25 °C). In Fig. 13 we can observe, as for the smaller *n*-alkane (Fig. 8), a very strong correlation between the relaxation of the $\mathbf{e}_1$ vector and the average result for the two equivalent **c** vectors at the center of the isoparaffine (where no branches are present). The relaxation curves of the

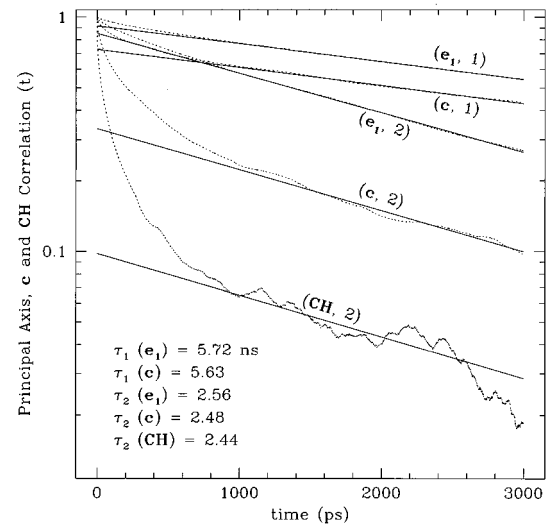

FIG. 13. Comparison of global (first- and second-order) rotational relaxation ($\mathbf{e}_1$) and local backbone reorientation (**c**) in squalane. We find τ_1/τ_2 ratios of 2.23 and 2.27 for the $\mathbf{e}_1$ and the **c** vectors, respectively. Second-order **CH** bond reorientation is also shown. The local vectors reflect the relaxation at the center of the molecule.

global and local backbone orientation track each other after a transient which is also 2 orders of magnitude longer for squalane (≈1 ns) than for *n*-decane (≈10 ps). In the same picture, we also show the second-order relaxation of the central **CH** vectors. Here, however, because of the limited time range available and the level of noise, only a qualitative comparison is possible.

We can see two possible reasons for the this correlation. For short alkanes (as *n*-decane or smaller) the intrinsic rigidity of the individual molecule, that is the presence of strong orientational correlations along the entire length of the molecule's backbone, can play a major role. The presence of a correlation between local and global reorientation in longer molecules (evident away from the two end-regions) may, on the other hand, suggest that both global and local molecular orientations are subject to the same intermolecular constraints. It would be interesting to test this idea by repeating the same analysis for long molecules in solution.

VI. CONCLUSIONS

We have shown that united atoms models can be useful for a quantitative understanding of the dynamical behavior of medium size alkanes. In the region of phase space investigated, model *B* was shown to provide a very good description of the transport properties of *n*-alkanes. Possible limitations of this model with regard to equilibrium properties were also pointed out. While significant differences were noticed in the calculated diffusion constants for the different models investigated, the more striking differences were observed in the local intrachain relaxation behavior. It was also shown that, for all models and structures considered, a correlation exists between the global rotational relaxation of the molecule and the relaxation of the local backbone orientation in the central region of the molecule. It would appear that ^{13}C NMR is a particularly valuable tool for investigating some of these issues.[29] At the shorter time scales, different choices of model potentials could be discriminated by their effect on local dynamics, while, at longer time scales, we might gain insight into the relation between the local and global orientational dynamics of the molecule.

We should stress the need for an improved set of UA LJ parameters for branched alkanes and we are presently trying to develop a systematic approach to this problem. We have already pointed out the limitations of our present model with respect to the PVT behavior of squalane (see Sec. III), we should also add that, because of the numerous methyl side-groups present in the the molecule, the internal cohesive energy of the isoparaffine will also be significantly overestimated.[7] The results presented, however, show that our model reproduces reasonably well the temperature dependence of the self-diffusion coefficients of *n*-tetracosane and squalane and we are now in a position to further investigate the relation between the two molecular structures and the significant difference observed in the temperature dependence of diffusion (and viscosity). To gain a more complete picture of the effect of molecular structure, we are also extending our study to alkanes with longer side branches and star type molecules.

ACKNOWLEDGMENT

We thank A. Garcia and B. Silbernagel for helpful discussions and sharing their data.

[1] Lubricants are dewaxed to improve their low-temperature properties: Wax, if left in lubricant oils, causes them to thicken excessively in cold weather conditions.
[2] J. I. Siepmann, S. Karaborni, and B. Smit, Nature **365**, 330 (1993); B. Smit, S. Karaborni, and J. I. Siepmann, J. Chem. Phys. **102**, 2126 (1995).
[3] P. Padilla and S. Toxvaerd, J. Chem. Phys. **95**, 509 (1991).
[4] G. Reiter *et al.*, J. Chem. Phys. **101**, 2606 (1994).
[5] Note, however, that because of the different analytic form of the bending potential, the characteristic frequency of bending vibration is increased by 10% in our model *B* with respect to the value in Ref. 3.
[6] W. L. Jorgensen, J. D. Madura, and C. J. Swenson, J. Am. Chem. Soc. **106**, 6638 (1984).
[7] A comparison between calculated and experimental cohesive energies of small branched alkanes [M. Mondello (unpublished)] clearly shows that in this model the strength of the methyl groups LJ interaction is overestimated.
[8] In particular, an NVT simulation of squalane at 20 °C, using the experimental density and the optimized intermolecular potential function for liquid hydrocarbonse (Ref. 6) (including bond bending), lead to an equilibrium pressure of −90 MPa, more negative than for our nonoptimized model.
[9] These are X–CH–CH–Y, X–C–CH_2–Y, X–C–CH–Y, and X–C–C–Y.
[10] Y. Wang, K. Hill, and J. G. Harris, J. Chem. Phys. **100**, 3276 (1994).
[11] H. Berendsen *et al.*, J. Chem. Phys. **81**, 3684 (1984).
[12] H. Andersen, J. Comput. Phys. **52**, 24 (1983).
[13] This corresponds to the smallest eigenvalue of the inertia tensor and the associated eigenvector defines the direction of the longest principal axis of the molecule's ellipsoid of inertia.
[14] A. Boothroyd, A. R. Rennie, and C. B. Boothroyd, Europhys. Lett. **15**, 715 (1991).
[15] P. Pant, J. Han, G. Smith, and R. Boyd, J. Chem. Phys. **99**, 597 (1993).
[16] K. Honnell, C. Hall, and R. Dickman, J. Chem. Phys. **87**, 664 (1987).
[17] A. Garcia and B. Silbernagel (unpublished).
[18] F. Bachl and H.-D. Lüdemann, Z. Naturforsch. **41a**, 963 (1986).
[19] This is due to the fact that an increase (decrease) in σ will increase (decrease) pressure and decrease (increase) diffusion, while an increase (decrease) in ϵ will decrease (increase) both.
[20] This is only an approximate result and it does not imply that the diffusion process can be properly thought of as an activated (solidlike) process. No evidence of jumplike motion was found in the simulation.
[21] G. W. Nederbragt and J. W. M. Boelhouwer, Physica **13**, 305 (1947).
[22] A similar shift between the atomic and molecular temperatures was reported by J. G. Harris, J. Phys. Chem. **96**, 5077 (1992). This seems to be caused by a tendency of the RATTLE algorithm to underestimate the magnitude of the corrected (atomic) velocities. This effect also leads to a very slow decrease of the total energy in microcanonical simulations. An analogous effect in the SHAKE algorithm, on which the RATTLE algorithm is based, was pointed out by W. F. van Gunsteren and H. J. C. Berendsen, Mol. Phys. **45**, 637 (1982).
[23] J. Dymond and K. Harris, Mol. Phys. **75**, 461 (1992).
[24] Note that this effect would be considerably smaller if we assumed a $\sqrt{T}$ dependence of self-diffusion at constant density as in hard spheres. The main effect comes from the small temperature dependence of the prefactor, which would imply a temperature-dependent hard sphere radius.
[25] P. Debye, *Polar Molecules* (Dover, New York, 1929).
[26] B. Berne and R. Pecora, *Dynamic Light Scattering* (Wiley, New York, 1976).
[27] H. Takeuchi and R.-J. Roe, J. Chem. Phys. **94**, 7446 (1991).
[28] Systematic uncertainties in the estimated values of τ_1 and τ_2 are introduced by the presence of short-time and long-time deviations from purely exponential relaxation, see Sec. V.
[29] G. D. Smith and D. Y. Yoon, J. Chem. Phys. **100**, 649 (1994); G. D. Smith, D. Y. Yoon, W. Zhu, and M. D. Edinger, Macromolecules **27**, 5563 (1994).
[30] P. Padilla and S. Toxvaerd, J. Chem. Phys. **94**, 5650 (1991).
[31] API 42, *Properties of Hydrocarbons of High Molecular Weight* (American Petroleum Institute, Research Project 42, Washington, D.C., 1966).
[32] M. Gehrig and H. Lentz, J. Chem. Thermodynamics **15**, 1159 (1983).
[33] Aldrich, *Catalog Handbook of Fine Chemicals* (Aldrich Chemical Co., Milwaukee, WI, 1994).